Phase-field simulation of peritectic solidification closely coupled with directional solidification experiments in an Al–36 wt% Ni alloy

2009 J. Phys.: Condens. Matter 21 464112

(http://iopscience.iop.org/0953-8984/21/46/464112)

J. Phys.: Condens. Matter **21** (2009) 464112 (6pp) doi:10.1088/0953-8984/21/46/464112

Phase-field simulation of peritectic solidification closely coupled with directional solidification experiments in an Al–36 wt% Ni alloy

R Siquieri[1], E Doernberg[2], H Emmerich[1] and R Schmid-Fetzer[2]

[1] Center for Computational Engineering Science and Institute of Minerals Engineering, RWTH Aachen University, D-52056 Aachen, Germany
[2] Institute of Metallurgy, Clausthal University of Technology, Robert-Koch-Straße 42, D-38678 Clausthal-Zellerfeld, Germany

E-mail: siquieri@ghi.rwth-aachen.de, evelyn.doernberg@tu-clausthal.de, emmerich@ghi.rwth-aachen.de and schmid-fetzer@tu-clausthal.de

Received 7 May 2009, in final form 7 June 2009
Published 27 October 2009
Online at stacks.iop.org/JPhysCM/21/464112

Abstract
In this work we present experimental and theoretical investigations of the directional solidification of Al–36 wt% Ni alloy. A phase-field approach (Folch and Plapp 2005 *Phys. Rev.* E **72** 011602) is coupled with the CALPHAD (calculation of phase diagrams) method to be able to simulate directional solidification of Al–Ni alloy including the peritectic phase Al_3Ni. The model approach is calibrated by systematic comparison to microstructures grown under controlled conditions in directional solidification experiments. To illustrate the efficiency of the model it is employed to investigate the effect of temperature gradient on the microstructure evolution of Al–36 wt% Ni during solidification.

(Some figures in this article are in colour only in the electronic version)

1. Introduction

In spite of their appearance in many metallic systems, peritectic solidification reactions and the associated microstructure development are much less understood than single-phase or eutectic solidification reactions [1, 2]. Recently, considerable research efforts have been dedicated to developing alloys with intermetallic phases in search of improved material characteristics such as high strength, high ductility and high corrosion resistance at elevated temperatures. Many of these materials are produced by peritectic solidification reactions, such as in carbon steels, Cr–Ni stainless steels, copper alloys, magnetic and superconducting materials. The formation of a specific microstructure, determining these material characteristics, depends on a complicated interplay between initial material composition, imposed temperature gradients, growth velocity and, if present, convection in the melt [3]. Therefore it is not surprising that a wide variety of microstructures can be formed impacting on materials processing and production.

In this work the microstructure evolution in peritectic systems is investigated. An approach was taken which combines the efficiency of computer simulation with carefully controlled experimental work. The binary Al–Ni alloy system has been chosen as a model system for this investigation. In particular the peritectic reaction $L + Al_3Ni_2 = Al_3Ni$ and an alloy composition of 36 wt% Ni have been chosen for the first round of experimentation, presented in this paper. St John [4] classifies this peritectic reaction as type III, in which the absolute values of the slopes of the Al_3Ni phase boundaries are equal, and it has been chosen for its simplicity and experimental accessibility.

For about two decades the development of aluminium-based alloys has been accelerated, through extensive use of computer simulations in two main directions: development of existing aluminium alloys and creation of new groups of aluminium alloys. In all cases, advanced modelling tools for manufacturing processes and fundamental data are necessary.

Modelling and simulation of microstructure development during solidification has recently developed as a powerful tool to accompany carefully designed experiments. This kind of modelling sheds new light on the precise interaction of transport mechanisms, kinetics and nonlinear dynamic effects such as segregation to predict the precise solidification paths and any quantity related to these [5, 6].

In the last two decades phase-field models could establish themselves successfully as a most relevant simulation technique for the above problems. These models [7] deliver a high-resolution calculation of the microstructure development during solidification on a scale of several micrometres. In recent years several models based on the phase-field method have been developed with the goal of improving the quantitative conformity with experiments, especially in states close to the thermal equilibrium. Of special interest were, amongst others, their thermodynamic consistency [7, 8], questions of algorithmic efficiency [9], as well as the control of thermodynamic fluctuations [10, 11]. In order to also take the macroscopic length scale of the relevant transport fields which drive phase transformation and microstructure formation into account, the phase-field approach was successively combined with homogenization approaches [10, 11].

Simulations based on the phase-field approach have led to an increasingly precise understanding of nonlinear microscopic processes, which influence the forming of microstructures in the interplay with segregation, transport, phase transitions and kinetics. It has been proven to be somewhat more complicated to extend these models to include precipitations as well. One aspect that may limit the usefulness of phase-field models is the experimental uncertainty concerning values for some model parameters, e.g. interface energies and diffusion coefficients. These parameters are subject to intensive experimental research at present.

In order to simulate peritectic solidification of Al–Ni alloys, a previously developed quantitative phase-field model has been adapted and extended to the Al–Ni alloy system. It has been calibrated by systematic comparison to microstructures grown under controlled conditions in directional solidification experiments. To illustrate the efficiency of the model it has been employed to investigate the effect of temperature gradient on the microstructure evolution of Al–36 wt% Ni during solidification. We believe that this combination of phase-field simulation closely coupled with directional solidification experiments is most suited to the investigation of peritectic microstructure evolution and the factors affecting it. The advantages arise from an iterative approach where, once calibrated on the first experimental results, the simulation can be used to predict those factors, which will most strongly affect the solidification microstructure. This, in turn, reduces the experimental effort required in order to verify those results.

2. Model description

In the following we extend the phase-field model described in [6] to simulate directional solidification of the Al–36 wt% Ni alloy. We use three phase-field variables, with $p_i \in [0, 1]$ and $p_1 + p_2 + p_3 = 1$. We denote $\vec{p} \equiv (p_1, p_2, p_3)$ and we define p_1 for the Al_3Ni_2 phase, p_2 for the Al_3Ni phase and p_3 for the liquid phase, respectively.

The model approach is based on the free energy functional of a representative volume of the investigated material system, which is given by

$$F = H \int_V \left[\sum_i \frac{W(\theta_i)^2}{2} (\nabla p_i)^2 + f(p_i, c, T) \right] \mathrm{d}V \qquad (1)$$

where $W(\theta_i) = W_0(1 + \varepsilon_{p_i} \cos 4\theta_i)$ is the interface thickness, which depends on the orientation of the solid–liquid interface [12], with $\theta_i = \arctan \partial_y p_i / \partial_x p_i$ and ε_{p_i} being a measure of the anisotropy[3]. The constant W_0 is defined as $W_0 = \sqrt{K/H}$.

The free energy density $f(p_i, c, T)$ is

$$f(p_i, c, T) = \sum_i p_i^2 (1 - p_i)^2 + \tilde{\lambda} \left[\sum_i f_{c,i}(c, T) g_i(\vec{p}) \right], \qquad (2)$$

where $\tilde{\lambda}$ is a coupling constant given by

$$\tilde{\lambda} = \frac{X}{H},$$

where H and X are constants with dimensions of energy per unit volume and K being a constant with dimension of energy per unit length. The constant X is the dimensional prefactor of the concentration term and it sets the magnitude of the thermodynamic driving forces [6]. The constants K and H are constants that can be changed in order to achieve the desired surface tension and interface thickness.

The surface tension of an i–j interface is given by $\sigma_{i,j} = \frac{\sqrt{2}}{3} W H$.

The function $g_i(\vec{p})$ couples the phase-field to the concentration and the temperature.

The function $f_{c,i}(c, T)$ is the local Gibbs energy function, which is constructed using the CALPHAD method [13]. In this method the Gibbs energy of each phase is described with an appropriate mathematical model and adjustable parameters are optimized with the help of phase equilibrium and thermochemical data obtained from experimental measurements. While the authors recognize a necessity for further refinement of the thermodynamic description of the Al–Ni system, the current phase-field simulation is based on the work of Huang *et al* [14]. In order to perform numerical calculations in a strictly binary system, the Gibbs energy function of the Al_3Ni_2 phase has been simplified to exclude the contribution of thermodynamic vacancies.

To impose a fixed temperature gradient along the y direction we assume that the temperature field is independent of the interface position. This is done by assuming equal heat conductivities in all the phases. Thus the temperature field is given by

$$T = T_R + G(y - v_p t) \qquad (3)$$

where G is the temperature gradient, v_p is the pulling velocity and T_R is a reference temperature.

[3] Here we consider ε_{p_2} always equal to zero.

The dynamics of the phases are derived from the free energy functional F as

$$\tau(\vec{p})\frac{\partial p_i}{\partial t} = -\frac{1}{H}\frac{\delta F}{\delta p_i}, \tag{4}$$

where $\tau(\vec{p})$ is a relaxation time. In this work we neglect interface kinetics (small undercooling).

The conserved concentration field is given by

$$\frac{\partial c}{\partial t} + \vec{\nabla}\cdot\vec{J} = 0, \tag{5}$$

where $\vec{J}$ is the flux of the scaled concentration:

$$\vec{J} = -M(\vec{p})\vec{\nabla}\frac{\delta F}{\delta c}, \tag{6}$$

with $M(\vec{p})$ being a phase-dependent mobility.

The set of equations (3)–(6) are made dimensionless by using W as the length scale and τ as the time scale [11, 15]. The equations are discretized using a finite difference approach. We use second-order discretization for the high order terms and central difference discretization for the low order terms. The phase-field and the concentration equation are solved using an Euler explicit scheme.

As part of the optimization/implementation procedure we compute equation (4) for p_1 and p_2 only and use the fact that $p_3 = 1 - p_1 - p_2$ to identify the liquid phase.

In this way, the model approach described in this section can be used to simulate directional solidification of the Al–Ni alloy near the intermetallic phase Al_3Ni.

3. Experimental approach

The fabrication of a peritectic microstructure grown under known and controlled solidification conditions is no trivial task. First, an alloy within the peritectic composition range must be cast into cylindrical samples, aiming at a fine microstructure without macrosegregation. These samples are then remelted and solidified in a controlled Bridgman-type directional solidification experiment.

An alloy composition of Al–36 wt% Ni was chosen and prepared in bulk form from 99.99% pure aluminium (HYDRO Aluminium Deutschland GmbH, Bonn, Germany) and 99.97% pure nickel (ChemPur, Karlsruhe, Germany). Nickel has a much higher density than aluminium and also dissolves quite slowly in the aluminium melt. In order to achieve a homogeneous melt, the alloy was fabricated in a 120 kW, 3 kHz induction furnace, where a high degree of mixing is guaranteed by electromagnetic agitation. A ZrO_2 coating prevented reaction between the melt and the graphite induction crucible. The graphite crucible was open to ambient atmosphere. After melting at 1100 °C for 20 min, the melt was cast into a steel permanent mould, thus achieving rapid cooling.

In the next stage of sample preparation, small amounts of the alloy were remelted and vacuum cast into silica tubes with an inner diameter of 7 mm, a wall thickness of 1 mm and a length of 330 mm. The advantage of using silica tubes in the vacuum casting process is their temperature shock resistance. This ensures that the top end of the tube, which is cooled, does not break when the hot melt rises due to the applied vacuum while the bottom end is immersed in the melt. Because silica reacts strongly with molten aluminium, the tubes were first coated with a boron nitride (BN) suspension.

The silica tubes cannot be used in the Bridgman experiment, where the sample must be held above 960 °C, the melting point of the alloy, since, in addition to the reactivity, silica does not remain mechanically stable for longer periods at this temperature. The vacuum-cast metal rods were consequently removed from the silica tubes, cleaned of any BN debris and inserted into thin-walled (0.5 mm) alumina tubes with a 7 mm inner diameter. These tubes were then sealed at the base with ceramic cement, before being used in the Bridgman experiment.

A new Bridgman apparatus was constructed specifically for this work. It is a simple but effective apparatus consisting of a vertical tube furnace with two separately controllable heating sections, a cooling basin with continually cycled water and an optimized jet of cooling water aimed at the immersed cold end of the sample tube. A precision motor with continually variable speed is used for the controlled lowering of the sample through the furnace and into the cooling basin. The design of this apparatus is based on previous experience within the research group on the directional solidification of magnesium alloys [16].

The magnitude of the temperature gradient (G) in the sample is controlled by adjusting the temperature in the lower section of the furnace, as well as adjusting the height of an insulating baffle between the furnace and the cooling basin. The solidification rate (v) can be adjusted simply by varying the speed of the motor used for lowering the sample. The motor has an analogue controller and the exact driving time and distance were measured for each experiment. The solidification rates used during this work varied from $v = 100$ to 400 μm s^{-1}. The temperature gradients used were measured in separate experiments where a thermocouple was inserted in a dummy sample. By adjusting the configuration of the Bridgman apparatus temperature gradients of $G = 8$, 13 and 17 K mm^{-1} were used for this work. This converts to a range of cooling rates (GV) between 0.8 and 6.8 K s^{-1}.

4. Results

The phase-field model above, associated with experimental investigation, allows us to numerically simulate directional solidification of Al–36 wt% Ni.

The simulation set up starts with a piece of Al_3Ni_2 phase in a supersaturated melt (see figure 1). The width of the simulation box (perpendicular to the growth direction) is chosen equal to the experimentally determined primary dendrite arm spacing $\lambda_1/2$. To reduce calculation time and memory consumption the investigations were optimized by simulating only half of a dendrite. To be able to simulate the whole dendrite structure we shifted the peritectic temperature to a value about 70 K above the original one.

The phase Al_3Ni_2 is allowed to grow until a time where it is relaxed. Once the phase Al_3Ni_2 is relaxed, a piece of the

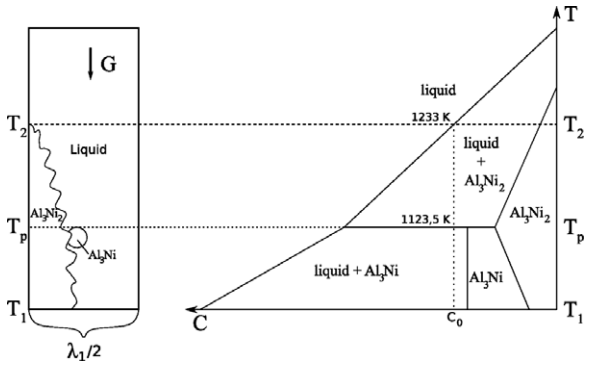

Figure 1. Schematic phase diagram and simulation set-up.

Al_3Ni phase is nucleated on the interface of liquid + Al_3Ni_2 and below the peritectic temperature, T_p. Note that we follow the solidifying front by advancing the simulation box from time to time along the growth direction. In practice, this is implemented by shifting the whole structure forward a distance equal to five grid spacings each time the product $v_p t$ of the pulling speed and time corresponds to a multiple of this distance [6, 11]. Basically, we follow the growth near the peritectic temperature. The simulation window, which we use for the simulation set-up, corresponds to the temperature range containing the peritectic temperature. The assumed nucleation temperature was 80 K below T_p. This causes the peritectic phase to grow both along the Al_3Ni_2 + liquid interface and inside the liquid phase.

Because of the number of unknown physical parameters for the studied system a calibration of the models with the experiments is necessary. In order to calibrate/validate the model, there are two aspects to be considered. First, one needs real solidification microstructures of the model alloy system. These microstructures should be obtained under well-controlled solidification conditions. The second important aspect is that in the simulation itself there are some parameters whose values are not precisely known. For instance, diffusion coefficients in the liquid and the anisotropy of the interface energy are two of these parameters.

The microstructure pictures taken from the solidification experiments were used for qualitative comparison with the numerical simulation. By performing parameter studies in a coordinate space where the diffusion coefficient of Al–Ni in the liquid and the anisotropy of the interface energy are the main coordinates, one may observe how the morphology (dendrite tip radius and secondary arm spacing) depends on these 'free' parameters. Of course, although the values of these parameters are not exactly known, there is a reasonable range for their variation, from a physical standpoint (in the case of the diffusion coefficient we use a constant value, which was based on computed values described in [17]). Following such a parameter study the diffusion constant in the liquid was selected as $D_L = 1.0 \times 10^{-9}$ m^2 s^{-1} and the anisotropy of the properitectic phase as $\varepsilon_4 = 0.05$. The diffusion constant in the solid phase was taken as $D_S = 1.0 \times 10^{-10}$ m^2 s^{-1}. The surface tension was assumed to be equal in both solid phases. It was taken to be $\sigma_{i,L} = 0.09$ J m^{-2}, which is also an estimated value.

After accomplishing this parameter study, we defined which set of parameters give a reasonable agreement between the experimental microstructure and the simulation. The results are compared in figure 2.

The value of the secondary arm spacing from the experiment, λ_2, was approximately 38 μm. From the simulation, λ_2 was determined as having the value of 22 μm. The values are of the same order of magnitude and within an acceptable range for the first stage of modelling. In figure 2, on the left, one can observe the Al_3Ni_2 phase after quenching the structure of a dendrite tip at the top of the mushy zone. The simulation on the right side also shows the dendritic structure for the same alloy at a height in the mushy zone where the Al_3Ni phase starts to form. The nucleation was described by supposing that a nucleus forms at a certain critical undercooling. The critical undercooling for the peritectic (Al_3Ni, mid-grey phase) nucleation was set at a high value. This caused the primary dendrite from the simulation to get much thicker than the corresponding experimental one.

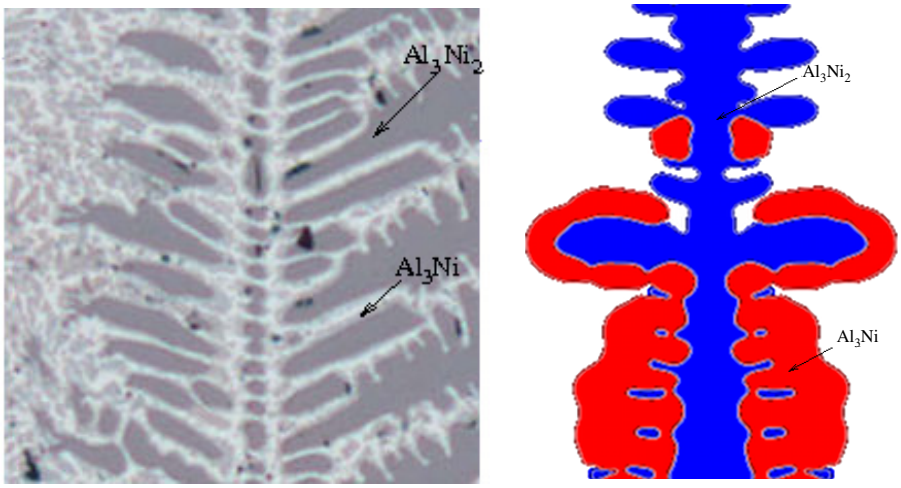

Figure 2. Comparison between experimental and simulated microstructure. Dark grey = Al_3Ni_2 and mid grey = Al_3Ni. Both pictures correspond to a box of 400 μm × 400 μm.

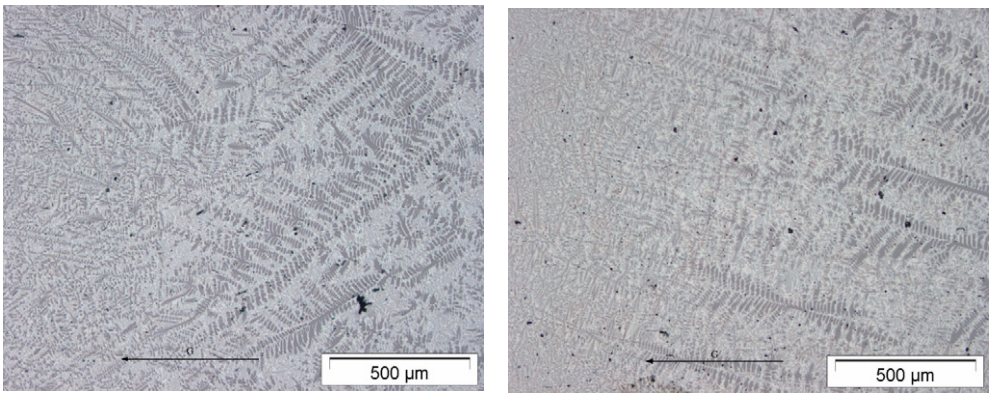

(a) (b)

Figure 3. Dendrite tips at the outset of the mushy zone for (a) $G = 13$ K mm^{-1} and (b) $G = 20$ K mm^{-1} at the same pulling velocity $v = 100$ μm s^{-1}. Al_3Ni_2: dark, Al_3Ni: mid, Al_3Ni/(Al)-fcc eutectic: light.

After calibrating the phase-field model, it can be used to conduct a systematic investigation of directional solidification for the system Al–36 wt% Ni. The fixed physical parameters, for instance, anisotropy of the interfacial energy and diffusion constant in the liquid, were used in all the simulations. An average value for the primary dendrite spacing was determined based on different experimental microstructures. This value was used in all the simulations ($\lambda_1 = 400$ μm).

Figure 3 shows a typical dendritic microstructure obtained by the Bridgman experiment. The figure shows the solidification front for (a) $G = 13$ K mm^{-1} and (b) $G = 20$ K mm^{-1} at the same pulling velocity $v = 100$ μm s^{-1}.

Observe that at the dendrite tips a large amount of unreacted Al_3Ni_2 dendrites can be seen. Thus the residual melt, which has solidified rapidly between the dendrite arms, is poor in Ni and solidifies to form only Al_3Ni and the eutectic structure. The melt, which remains beyond the solidification zone (on the left in each micrograph in figure 3) has the same overall composition of the alloy, namely Al–36 wt% Ni, and thus solidifies during quenching to form a fine structure including the properitectic Al_3Ni_2 phase.

As observed in figure 3, not much difference can be seen when the temperature gradient is changed from 13 to 20 K mm^{-1}. Due to experimental difficulties a larger temperature gradient was not possible to be investigated. Nevertheless, we conducted numerical simulation for a much larger range of temperature gradients. The temperature gradient was tested from $G = 20$ to 100 K mm^{-1}.

In figure 4 we simulate the time evolution of directional solidification for Al–36 wt% Ni with process parameters similar to the ones used in figure 3(b), namely $G = 20$ K mm^{-1} and $v = 100$ μm s^{-1}. The critical temperature for nucleation of the peritectic phase was set at 4 K below the peritectic temperature. The reference temperature for the position of the dendrite tip was set in a way that the dendrite can fully develop with side branches. Observe that after nucleation the peritectic phase grows around the properitectic phase, but it also grows into the properitectic phase as well as into the liquid. In the last figure on the right-hand side of figure 4 you can see that some side branches of the properitectic phase were almost completely consumed from the peritectic phase.

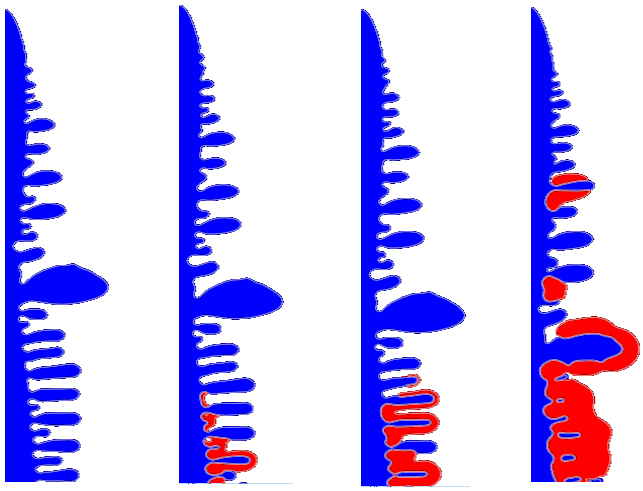

Figure 4. Growth of peritectic intermetallic phase from the dendritic Al_3Ni inside the mushy zone. Time evolves from left to right. We use $G = 20$ K mm^{-1} and $v = 100$ μm s^{-1}. Dark grey represents the dendritic phase Al_3Ni_2 and mid-grey the Al_3Ni phase.

Next we increase the temperature gradient while the pulling speed remained constant $v = 100$ μm s^{-1}. The tests were done for $G = 30$, 50, 80 and 100 K mm^{-1}. As we increase the temperature gradient we note a structural refinement. The dendritic structure becomes finer and the value of the primary dendrite space λ_1 becomes smaller. Work on a systematic investigation of the effect of process condition on the primary dendrite space during the solidification of the Al–Ni alloy is in progress. To illustrate these observations in figure 5 we show the time evolution simulation of directional solidification for Al–36 wt% Ni using $G = 100$ K mm^{-1} and $v = 100$ μm s^{-1}. Note that the dendritic structure is finer than the one shown in figure 4. Again we let the phase Al_3Ni_2 grow until it is totally relaxed, then a piece of the phase Al_3Ni is nucleated on the interface liquid + Al_3Ni_2 and below the peritectic temperature. Observe that again the peritectic phase grows into the properitectic phase as well as into the liquid.

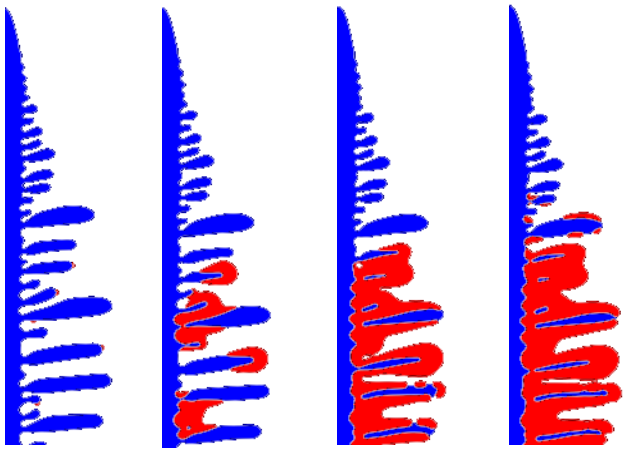

Figure 5. Growth of peritectic intermetallic phase from the dendritic Al_3Ni inside the mushy zone. Time evolves from left to right. We use $G = 100$ K mm^{-1} and $v = 100$ μm s^{-1}. Dark grey represents the dendritic phase Al_3Ni_2 and mid-grey the Al_3Ni phase.

5. Summary and discussion

Experimental and theoretical investigations of directional solidification of the Al–36%Ni alloy have been presented. An existent phase-field model is coupled with the CALPHAD method to be able to simulate directional solidification of the Al–Ni alloy including the intermetallic phase Al_3Ni. The model approach is calibrated by systematic comparison to microstructures grown under controlled conditions in directional solidification experiments.

After calibrating the model with the experiments, it was used to conduct a series of simulations where the temperature gradient was varied and the pulling velocity was kept constant. It was observed that the dendritic structure becomes finer with the increase of the temperature gradient and, as a consequence, the primary dendrite spacing decreases.

In order to improve the simulation results some further aspects still need to be included in the model. The first aspect is a further investigation of the heterogeneous nucleation kinetics during the peritectic growth and the inclusion of a nucleation model for the long-range interaction effects. The second aspect is that the microstructure is obviously three-dimensional and not two-dimensional. It may have an effect on the thermodynamics since the curvature of the interfaces between solid and liquid, which may be positive or negative, contributes to the local undercooling of the alloy, and this will have an effect on the concentration distribution, which can cause a strong influence on the nucleation and consequently on the microstructure evolution.

Moreover, the model approach developed in this paper can be used to obtain new relations between processing parameters and resulting kinetics and dynamics of the phase-transformation process. We believe that this combination of phase-field simulation closely coupled with directional solidification experiments is most suited to the investigation of peritectic microstructure evolution and the factors affecting it.

References

[1] Kerr H W 1996 *Int. Mater. Rev.* **41** 129
[2] Umeda T, Okane T and Kurz W 1996 *Acta Mater.* **44** 4209
[3] Lograsso T A, Fuh B C and Trivedi R 2005 *Metall. Mater. Trans.* A **36** 1287
[4] St John D H and Hogan L M 1987 *Acta. Metall.* **35** 171
[5] Steinbach I, Pezzolla F, Nestler B, Seeßelberg M, Prieler R, Schmitz G J and Rezende J L L 1996 *Physica* D **94** 135
[6] Folch R and Plapp M 2005 *Phys. Rev.* E **72** 011602
[7] Emmerich H 2003 *The Diffuse Interface Approach in Material Science—Thermodynamic Concepts and Applications of Phase-Field Models* (*Springer Monograph, Lecture Notes in Physics*) (Berlin: Springer) p 73
[8] Emmerich H 2003 *Contin. Mech. Thermodyn.* **15** 197
[9] Hubert J and Emmerich H 2005 *Fortschritte in der Simulationstechnik ASIM* (Erlangen: SCS Publishing House)
[10] Emmerich H, Jurgk M and Siquieri R 2004 *Phys. Status Solidi* b **241** 2128
[11] Siquieri R and Emmerich H 2009 *Steel Res.* **1** 9
[12] Karma A and Rappel W-J 1996 *Phys. Rev.* E **53** R3017
[13] Lukas H L, Friers S G and Sundman B 2007 *Computational Thermodynamics: The Calphad Method* (Cambridge: Cambridge University Press)
[14] Huang W and Chang Y A 1998 *J. Phase Equilib.* **19** 25
[15] Siquieri R and Emmerich H 2007 *Phil. Mag. Lett.* **87** 829
[16] Mirković D and Schmid-Fetzer R 2009 *Metall. Mater. Trans.* A **40** 958
[17] Kerrache A, Horbach J and Binder K 2008 *Eur. Phys. Lett.* **81** 58001